HHS Public Access

Author manuscript

Dev Cell. Author manuscript; available in PMC 2023 April 25.

Published in final edited form as:

Dev Cell. 2022 April 25; 57(8): 1068–1080.e6. doi:10.1016/j.devcel.2022.03.013.

Rapid and efficient degradation of endogenous proteins *in vivo* identifies stage specific roles of RNA Pol II pausing in mammalian development

Abderhman Abuhashem[1,2,3], **Andrew S. Lee**[1,4], **Alexandra L. Joyner**[1,3,4], **Anna-Katerina Hadjantonakis**[1,3,5,*]

[1]Developmental Biology Program, Sloan Kettering Institute, Memorial Sloan Kettering Cancer Center, New York, NY, 10065, USA

[2]Weill Cornell/Rockefeller/Sloan Kettering Tri-Institutional MD-PhD Program, New York, NY, 10065, United States

[3]Biochemistry Cell and Molecular Biology Program, Weill Cornell Graduate School of Medical Sciences, Cornell University, New York, NY 10065, USA

[4]Neuroscience Program, Weill Cornell Graduate School of Medical Sciences, Cornell University, New York, NY 10065, USA

[5]Lead contact:

SUMMARY

Targeted protein degradation methods offer a unique avenue to assess a protein's function in a variety of model systems. Recently, these approaches have been applied to mammalian cell culture models, enabling unprecedented temporal control of protein function. However, the efficacy of these systems at the tissue and organismal levels *in vivo* is not well established. Here, we tested the functionality of the degradation tag (dTAG) degron system in mammalian development. We generated a homozygous knock-in mouse with a $FKBP12^{F36V}$ tag fused to Negative elongation factor b (*Nelfb*) locus, a ubiquitously expressed regulator of transcription. In our validation of targeted endogenous protein degradation across mammalian development and adulthood, we demonstrate that irrespective of the route of administration the dTAG system is non-toxic, rapid,

*Correspondence: hadj@mskcc.org.

AUTHOR CONTRIBUTIONS

A.A. and A.K.H. conceptualized the study. A.S.L. performed brain stereotaxic injections. A.A. performed all other experiments. A.A. analyzed and interpreted all data. A.A. wrote the original draft. A.A. wrote revised draft with input from all authors. A.A. and A.K.H acquired funding. A.K.H. supervised the work.

DECLARATION OF INTERESTS

A.K.H is on the advisory board for Developmental Cell. All other authors have no competing interests to declare.

INCLUSION AND DIVERSITY

One or more of the authors of this paper self-identifies as an underrepresented ethnic minority in science. One or more of the authors of this paper self-identifies as a member of the LGBTQ+ community. While citing references scientifically relevant to this work, we also worked to promote gender balance in our reference list.

and efficient in embryos from the zygote to mid-gestation stages. Additionally, acute depletion of NELFB revealed a specific role in zygote-to-2-cell development and Zygotic Genome Activation (ZGA).

Graphical Abstract

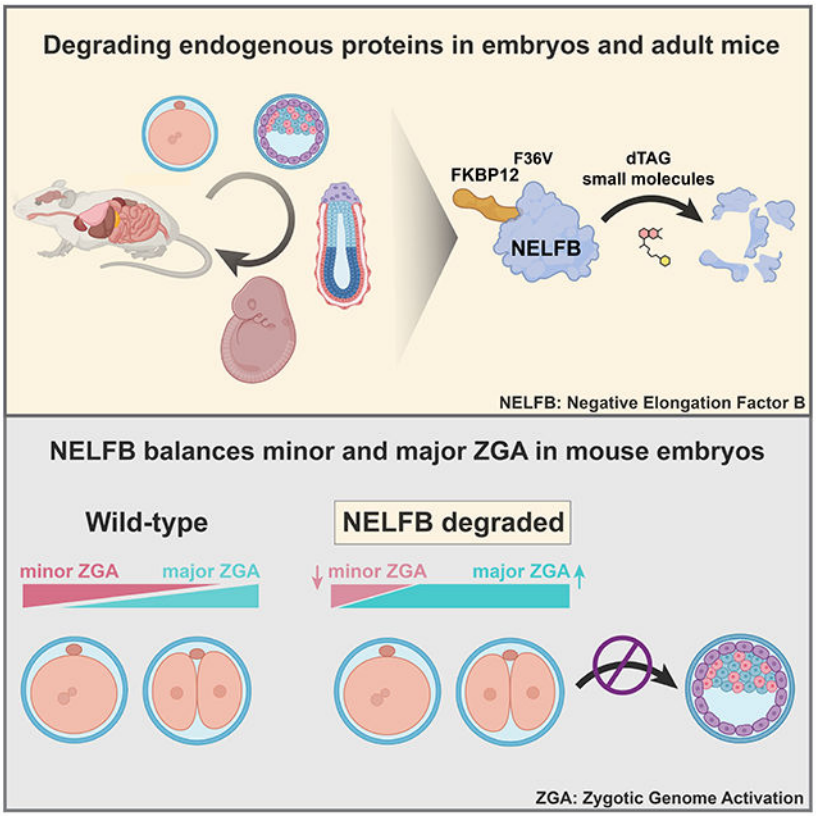

ETOC BLURB

Abuhashem et al. evaluate the kinetics and efficacy of the dTAG degron system *in vivo* in a mouse model. They find that the system is safe, inducible, efficient, and reversable across mammalian development and adult tissues. Using this system, they identify a function for RNA Pol II pausing in regulating mammalian zygotic genome activation.

Keywords

degron; dTAG; mouse embryo; pre-implantation; post-implantation; zygote; ZGA; NELF; pausing; transcription

INTRODUCTION

Molecular perturbation methods have been evolving rapidly over the last few decades and provide an invaluable tool to interrogate gene function across biological contexts. Broadly, these methods can be categorized based on their point of action: DNA, RNA, or protein.

The recent revolution in CRISPR systems enormously expanded the DNA/RNA targeting toolbox (Pickar-Oliver and Gersbach, 2019). However, because proteins are the functional biological units in the majority of contexts, targeting DNA/RNA poses several limitations. These include slow onset of effect and the possibility of adaptation, irreversibility when DNA is modified, and biological plasticity from alternative splicing (Smits et al., 2019; Verma et al., 2020; Wu et al., 2020). These limitations hinder experimental design and ultimately appropriate interpretation of protein functions in scenarios that require acute perturbation and/or reversibility.

Direct protein perturbation is an attractive alternative that may offer superior temporal resolution to DNA/RNA targeting methods (Wu et al., 2020). While small molecules can be used to target some proteins, the druggable proteome currently represents a small subfraction of proteins in a cell (Chamberlain et al., 2019). Recent development of degron approaches, such as the auxin-inducible degron (AID) and degradation tag (dTAG) systems offer the possibility of targeting any protein in a cell in a rapid, inducible, and reversable manner (Verma et al., 2020). These systems rely on genetic fusion of the gene of interest to a small tag. Upon introduction of a small molecule that binds specifically both the tag and ubiquitination proteins, the tagged protein can be directed for proteasomal degradation. These system have enabled discoveries in cell models that were not previously possible (Jaeger and Winter, 2021). Notably, the dTAG system exclusively relies on the mammalian endogenous proteasomal degradation machinery, while the AID system requires the expression of a exogenous plant-based factor to activate the system (Nabet et al., 2018; Nishimura et al., 2009). Despite their promise, it is unclear how safe or functional these systems are *in vivo*, particularly during mammalian development.

Early mammalian development poses a unique challenge for interrogation of protein function. During pre-implantation embryo development, maternally deposited transcripts can mask early loss of function (knockout) phenotypes, often necessitating generation of maternal/zygotic mutants through complex and imperfect Cre/loxP genetic systems that knockout both maternal and zygotic genes (Sun et al., 2008). Early post-implantation, Cre-estrogen receptor (CreER) systems can offer some spatio-temporal specificity, but often result in mosaic recombination across and within embryos, while tamoxifen injections can have teratogenic effects on embryos, as well as leading to implantation failure during these stages (Pimeisl et al., 2013; Savery et al., 2020; Ved et al., 2019). Thus, there is a need for a safe, efficient, rapid, inducible, and reversable perturbation system to probe gene functions in complex mammalian systems. Ideally, such a system would also enable iterative and/or successive interrogation of gene function at a variety of developmental stages.

Here, leveraging recent observations in mammalian cells and compelling safety and specificity profile, we sought to implement the dTAG system in mammalian embryos. We tagged Negative Elongation Factor-b (NELFB) with $FKBP12^{F36V}$ in mouse embryonic stem cells (mESCs). *Nelfb* is widely expressed across mouse development, enabling validation of the dTAG system at a wide range of stages (Nowotschin et al., 2019; Pijuan-Sala et al., 2019). Then, we used these mESCs to generate germline-transmitting mice. Resulting F1 animals heterozygous for the *Nelfb-FKBP12*^{F36V} allele were subsequently used to generate a homozygous mouse with this allele, demonstrating the fusion to be safe. Using

this *Nelfb-FKBP12*^{F36V} allele, we demonstrated that the dTAG system provides highly efficient acute protein degradation across pre- and post- implantation embryonic stages (E0.5 – E9.5). We found that dTAG small molecules dTAG-13 and dTAGv-1 are non-toxic during development and safe for use in *in vitro* embryo culture and via intraperitoneal injection into pregnant adult females. The system achieves maximum efficiency within one hour in *ex utero* cultured pre-implantation embryos, and within ~4 hours *in vivo* in post-implantation embryos. Furthermore, we show that the system is highly efficient across adult mouse tissues. We utilized the system to uncover a role for NELFB in pre-implantation development, specifically in zygotic genome activation (ZGA). We found that NELFB attenuates the initiation of major ZGA. Overall, we report successful adaptation of a degron system to perturb an endogenous protein in a mouse model during embryonic stages and adulthood.

DESIGN

We considered several degron systems for application in the context of mammalian embryonic development including the AID, dTAG, and TRIM-away systems (Clift et al., 2017; Nabet et al., 2018; Nishimura et al., 2009). While the TRIM-away system does not require gene editing as it relies on antibodies to identify target proteins, it can be technically challenging depending on the sub-cellular localization of the target protein and consequently antibodies, which are not cell permeable (Clift et al., 2017). Both the AID and dTAG systems offer comparable advantages in terms of acute degradation of a genetically edited tagged target protein (Nabet et al., 2018; Nishimura et al., 2009). The second iteration of the AID system, AID2, overcame significant challenges of basal degradation and has been shown to be effective in degrading a tagged transgene reporter *in vivo* in mice (Nishimura et al., 2020; Yesbolatova et al., 2020). However, auxin derivatives have been shown to be bioactive and can potentially affect embryonic development (Nishimura et al., 2020). Furthermore, all auxin systems require constitutive exogenous expression of a plant-based accessory protein (e.g. OsTIR1). By contrast, the dTAG system only requires editing a locus of interest to introduce a FKBP12^{F36V} tag. Additionally, several recently developed dTAG molecules (e.g. dTAG-13 and dTAGv-1) can induce degradation at nanomolar concentrations and do not appear to induce biological activity in the absence of the FKBP12^{F36V} tag (Nabet et al., 2018, 2020). Depending on the dTAG molecule used, either CRBN or a VHL-mediated proteasomal degradation is engaged, which can theoretically expand the functionality of the system to more cell types.

NELFB regulates a critical step in transcription, promoter-proximal RNA Pol II pausing. As a result, it is present across mammalian development and tissues (Nowotschin et al., 2019; Pijuan-Sala et al., 2019). It therefore represents an ideal choice of locus to assess the dTAG system across a variety of stages and tissues. Furthermore, the role of NELFB has not been assessed at early developmental stages and a recent study suggested a dynamic role for NELFB at the zygote/2-cell stages (Liu et al., 2020). These considerations motivated us to design a successful mouse model with degradable NELFB and to test its function at pre-implantation stages.

RESULTS

Generation of *Nelfb*^{dTAG} mouse to test the dTAG system *in vivo*

To assess use of the dTAG system *in vivo*, we sought to generate a mouse model harboring an endogenously tagged protein. To do so, we utilized CRISPR/Cas9 and homology-directed repair (HDR) to insert FKBP12^{F36V} in-frame at the C-terminus of NELFB by targeting the final coding exon 5' of the STOP and 3' UTR in mESCs (Figure S1A)(Nabet et al., 2018; Ran et al., 2013). Structural studies have shown that the c-terminus of NELFB is not involved in critical interactions of the protein (Vos et al., 2018a). The edited allele also included two HA tags to facilitate detection. mESC clones with correct integration of the tag at the *Nelfb* locus were identified by PCR (Figure S1B). To ensure that the tagged allele, *Nelfb*^{dTAG}, was properly expressed and translated, we performed immunofluorescence against the HA tag in a heterozygous clone, which showed robust nuclear staining as expected for NELFB (Figure 1B). Western blot analysis using an antibody against NELFB showed two bands separated by ~13kD, corresponding to the molecular weight of FKBP12^{F36V} (Figure 1C). The bands show similar intensities, suggesting that NELFB-FKBP12^{F36V} is stable in the absence of degradation promoting small molecules.

To test whether NELFB-FKBP12^{F36V} could be degraded, we treated cells with 500nM dTAG-13. dTAG-13 is a heterobifunctional small molecule that binds to the FKBP12^{F36V} tag and CRBN, resulting in rapid proteasomal degradation of the target protein (Figure 1A)(Nabet et al., 2018). As expected, NELFB-FKBP12^{F36V} was rapidly degraded to undetectable levels when assayed via western blot or immunofluorescence (Figure 1B and 1C). Notably, full degradation was achieved within 30 minutes of adding dTAG-13, reflecting the temporal advantages of the dTAG system in mESCs. To test whether these dynamics are titratable, we treated cells with varying concentration of dTAG-13 from 0.1 to 500nM and determined degradation efficiency by 30 mins. We found that using lower concentrations, 10nM, can induce ~60% degradation, while even lower concentrations resulted in minimal degradation within this time frame (Figure S1D). Thus, we find the system to be highly efficient and titratable in cells.

To generate a mouse with the *Nelfb*^{dTAG} allele, cloned heterozygous mESCs containing the correctly targeted insertion were injected into 8-cell embryos to generate germline transmitting chimeras (Figure S1C)(Poueymirou et al., 2007). To test whether the edited allele is expressed *in vivo*, we performed immunofluorescence staining of the HA tag in E7.5 embryos resulting from heterozygous, *Nelfb*$^{dTAG/+}$, and wild-type, *Nelfb*$^{+/+}$, crosses. These data showed that the *Nelfb*^{dTAG} allele is inherited at mendelian ratios and robustly expressed across heterozygous embryos, while HA staining is absent in wild-type embryos (Figure 1D). To further test the functionality of the tagged allele, heterozygous mice were crossed to generate homozygous *Nelfb*$^{dTAG/dTAG}$ mice. Heterozygous intercrosses resulted in viable and fertile homozygous animals that were indistinguishable from heterozygous and wild-type littermates, and were recovered at Mendelian ratios (Figure S1E). *Nelfb*$^{dTAG/dTAG}$ animals did not display any detectable phenotype and were able to generate normal sized litters (Figure S1F). The tagged allele did not show significant differences in expression assayed by RT-qPCR, and the tagged protein was expressed at comparable levels to wild-

type in heterozygous and homozygous mice (Figure S1G and S1H). Additionally, the expression of several genes that have been shown to have NELF binding at their promoters was not affected (Figure S1G)(Rahl et al., 2010). Furthermore, complementing a previously generated protein-null *Nelfb* allele with $Nelfb^{dTAG}$ resulted in viable and healthy animals (Figure S1I)(Williams et al., 2015). Of note, *Nelfb* has been shown to be required for post-implantation mammalian embryonic development, suggesting that $Nelfb^{dTAG}$ is functional (Amleh et al., 2009; Williams et al., 2015). These data support that we have generated a mouse model that widely expresses an endogenous NELFB-FKBP12^{F36V} fusion protein. This enables us to evaluate the dTAG system *in vivo* and to glean insights into the role of NELFB in early development.

The dTAG system is safe, efficient, and reversable in pre-implantation embryos

Mammalian pre-implantation development encompasses the time from fertilization to implantation of the embryo in the maternal uterine wall. During this period embryos grow independently from maternal tissues, and can be retrieved and routinely cultured *ex utero* (Piliszek et al., 2011). This flexibility has made pre-implantation embryos an excellent system to study a variety of biological processes in mice (Saiz et al., 2015). Before testing the efficiency of the dTAG system in pre-implantation embryos, we wanted to test whether dTAG-13 is toxic for culturing mouse embryos from the zygote until the late blastocyst stages *in vitro*. Wild-type zygotes were cultured *ex utero* for 96 hours in standard medium (KSOM) with or without 500nM of dTAG-13 (Figure 2A)(Behringer et al., 2014). Based on our mESC experiments and previous reports, we expected that this concentration of dTAG-13 would be sufficient to activate degradation in pre-implantation embryos (Nabet et al., 2018, 2020). We found that dTAG-13 had no effect on the developmental potential of zygotes which developed to the late blastocyst stage (Figure S2A and S2B). To examine whether the *ex utero* cultured blastocysts with or without dTAG-13 developed normally, they were fixed and immunostained for markers of distinct cell fates. Late stage blastocyst embryos normally contain three cell lineages: epiblast (marked by NANOG), primitive endoderm (marked by GATA6), and trophoblast (marked by CDX2) (Schrode et al., 2013). We found that blastocysts that were cultured in the presence of dTAG-13 contained all these lineages (Figure S2C). Additionally, we found that the total cell number, and the ratio of trophoblast to total cell number were preserved (Figure 2A). Taken together these data suggest that, at concentrations shown to promote degradation in other systems, dTAG-13 is non-toxic for pre-implantation development.

To test whether the dTAG system drives efficient degradation in pre-implantation embryos, we collected E3.5 blastocysts recovered from crosses of $Nelfb^{dTAG/+}$ males with wild-type females. This crossing strategy provided both negative and positive controls within each litter for comparable quantitative analyses. Blastocysts were cultured for 1 hr in KSOM with or without dTAG-13. Embryos were then fixed and immunostained for HA to detect NELF-FKBP^{F36V}. We found no detectable HA signal in treated $Nelfb^{dTAG/+}$ embryos, suggesting highly efficient and rapid degradation (Figure 2B, 2C and S2D). Of note, degradation was observed across the entire embryo, and did not spare certain cells based on fate or position. Similar results were observed for E4.5 blastocysts (Figure S2F). The treatment had no acute effect on total cell number per embryo (Figure S2E). Performing the same experiment at

finer temporal resolution, we noted that degradation was complete within 40 minutes of first exposure to dTAG-13 (Figure 2D). These results suggest that the dTAG system is efficient and can be used as an alternative strategy to conditional gene knockouts in pre-implantation embryos.

A key advantage of protein degradation approaches is their reversibility (Nabet et al., 2018). To test reversibility with the dTAG system in mouse pre-implantation embryos, E2.5 or E3.5 embryos were cultured in KSOM in the presence of dTAG-13 for 1 hr, followed by washing and culturing without dTAG-13 for various periods of time. Embryos were then fixed and immunostained for analysis. We found that the dTAG system is reversable within a few hours, with about 50% expression of degradable protein recovered in 5-8 hours (Figure 2D). We tested the reversibility dynamics using the minimal effective dose in blastocysts, 50nM, which did not differ from our initial treatment with 500nM (Figure S2G). While reversibility is slower than induction, and depends on additional factors such as levels of active gene expression, it is still rapid and outperforms other RNA-based systems such as RNAi (Verma et al., 2020). We speculate that the slower reversibility is in part due to potent binding of dTAG-13 to CRBN, thus requiring turnover of the protein to reverse the system. Taken together, these data show that the dTAG system is safe, rapid, efficient, and reversable in mouse pre-implantation embryos.

The dTAG system is safe, efficient, and reversable in post-implantation embryos

Post-implantation development commences once the embryo implants into the maternal wall. In mice, this period starts around day E5.0. Early post-implantation development is a crucial time with intricate processes taking place such as pluripotency exit, onset of gastrulation and the initiation of organogenesis which occur within a 48 hour period in mice (Bardot and Hadjantonakis, 2020). Inducible and tissue-specific knockout systems, for example those driven by the lineage-specific and/or inducible forms of the Cre recombinase, have enabled discoveries during these embryonic stages. However, induction in such systems can be mosaic, inducing recombination in only a proportion of cells, especially before E8.5, and can be highly teratogenic resulting in abortion and mothers' death (Pimeisl et al., 2013; Savery et al., 2020; Ved et al., 2019). These challenges make it difficult to generate inducible knockouts and study the consequences of acute protein loss during the early post-implantation period. Therefore, we aimed to test the safety and efficacy of the dTAG system at early post-implantation stages.

To test the toxicity of the dTAG system for post-implantation development, pregnant wild-type females received a single intraperitoneal (IP) injection of vehicle or dTAG-13 (35mg kg^{-1}) at 6.5dpc, 8.5dpc, or 10.5dpc and were then allowed to go to term to assess any developmental defects resulting from treatments. We found that all mice delivered healthy litters in numbers comparable to a control group (Figure S3A). This experiment was repeated with dTAGv-1, a recently developed small molecule that activates the dTAG system via the VHL degradation path and reported to have improved *in vivo* pharmacokinetics in comparison to dTAG-13 (Nabet et al., 2020). Similarly, we found that dTAGv-1 had no effect on the health of pregnant females or size of their litters (Figure 3A). Thus, when administered to pregnant females both dTAG-13 and dTAGv-1 are developmentally neutral

and non-toxic to use during post-implantation stages of development. Given the molecular differences and pharmacokinetics between dTAGv-1 and dTAG-13, we sought to include data on both in our following *in vivo* experiments.

Next, we wanted to test the efficiency of the dTAG system *in vivo* in post-implantation embryos. To do so, we delivered dTAG-13 or dTAGv-1 via IP injection to 6.5dpc pregnant females. After 4 hours, embryos were recovered, fixed, and stained. We found that a single injection of dTAG-13 or dTAGv-1 achieved complete and global degradation in E6.5 embryos (Figure 3B and 3C). To determine the dynamics of degradation, we performed the same experiment with females at 7.5dpc and collected embryos at 1, 2, 3, and 4 hours post injection. We observed >90% and >95% degradation was achieved within 3 and 4 hours respectively (Figure 3D and 3E). Similar results were obtained at mid-gestation stages when females at 9.5dpc were subject to a two-injection regime separated by 2 hours and followed for 6 hours post the second injection (Figure 3F and 3G). To determine whether the system is reversible *in vivo*, we injected animals with dTAG-13 or dTAGv-1 followed by a 24-hour chase before analysis. We found that expression was largely recovered at ~70% with dTAG-13 or dTAGv-1 (Figure S3B and S3C). These results are in agreement with known pharmacokinetics of dTAG small molecules (Nabet et al., 2020). Taken together, these data demonstrate the dTAG system to be efficient and reversible during post-implantation mouse embryo development *in vivo*.

The dTAG system is efficient and reversable in adult mouse tissues

We sought to assess the functionality of the dTAG system in adult mouse tissues. We found that a single IP injection of dTAGv-1 or dTAG-13 was sufficient to drive complete protein degradation within 6 hours in the liver, small intestine, lungs, and heart (Figure 4A and S4A). The degradation was also found to be reversible within 48 hours (Figure S4B). Notably, protein degradation was not detected in the brain, which is most likely protected from dTAG small molecules by the blood brain barrier (Figure 4A and S4A). To definitively test whether brain tissue is capable of degrading endogenous proteins using the dTAG system, we performed intracerebral injections of dTAGv-1 and dTAG-13 into the somatosensory cortex of *Nelfb*$^{dTAG/dTAG}$ mice. Indeed, we found that a direct injection resulted in complete degradation of NELFB-FKBP12^{F36V} within 2 hours at the site of injection (Figure 4B, 4C, and S4C). Of note, the dTAG molecules did not diffuse far from the injection site, and thus can be used to target specific brain regions or nuclei and the opposite side of the brain can be used as an internal control. Taken together, these data demonstrate the dTAG system to be efficient and reversible across adult mouse tissues including the brain, with the consideration that dTAGv-1 and dTAG-13 cannot traverse the blood brain barrier.

Acute degradation of NELFB reveals an essential role in pre-implantation development

Given the adaptability of the dTAG system to mammalian development and its unique, acutely inducible and reversable onset, we wanted to apply this system to a biological question that exploits these advantages. NELFB is an essential subunit of the negative elongation factor (NELF) complex (Yamaguchi et al., 1999). NELF has been shown to play a role in stabilizing transcriptionally engaged RNA Pol II at the promoter-proximal pausing

position (Kwak and Lis, 2013; Yamaguchi et al., 1999). Upon phosphorylation by CDK9, NELF is released from the paused polymerase, enabling binding of pro-elongation factors (Adelman and Lis, 2012; Vos et al., 2018c, 2018b). Pol II pausing has been shown to play an essential role in the regulation of gene expression across a variety of biological contexts (Abuhashem et al., 2022; Core and Adelman, 2019). In development, *Nelfb* knockout in mice results in embryonic lethality at early post-implantation in mice (Amleh et al., 2009). Furthermore, classical knockout strategies of essential genes cannot be used to examine whether a gene plays a role prior to the 4-8-cell stage in pre-implantation development, due to maternally deposited transcripts which can mask any potential phenotypes (Tadros and Lipshitz, 2009). A recent study has shown that Pol II pausing is uniquely prevalent in mouse embryos at the transition from zygote to 2-cell stages, coinciding with zygotic genome activation, or ZGA (Liu et al., 2020). Given that NELF subunits can be transcriptionally detected throughout pre-implantation mammalian development, we hypothesized that despite being dispensable for pre-implantation development after the 2-cell stage, NELF could play a critical role in ZGA.

To test this hypothesis, we first wanted to assess whether NELFB can be detected at the protein level in zygotes and 2-cell stage embryos. Previous analyses suggest that the *Nelfb* transcript is detected at low levels, but immunofluorescence studies have been inconclusive (Hu et al., 2020; Liu et al., 2020). We crossed homozygous $Nelfb^{dTAG/dTAG}$ males and females and collected zygotes at E0.5. Immunofluorescent staining for the HA tag revealed a signal localized to both maternal and paternal pro-nuclei (Figure 5B). Upon culture for 1 hour in dTAG, the signal was completely lost, suggesting degradation and activity of the dTAG system in zygotes (Figure 5A and 5B). Similar results were observed at the 2-cell stage (Figure 54A and 54B). The HA/NELFB staining at the zygote stage suggests that it is maternally deposited and expressed prior to ZGA. Because these embryos are the result of crossing homozygous mice, both maternal and zygotic transcripts are tagged, thus degradation ensures depletion of all protein present, regardless of the source.

To test whether NELFB plays a role in pre-implantation embryo development, we leveraged *ex utero* embryo culture between the zygote and blastocyst stages. To rigorously determine the safety of the dTAG system, we cultured wild-type and $Nelfb^{dTAG/+}$ embryos (derived from $Nelfb^{dTAG/+}$ mothers) in dTAG-13 for 96 hours, from the zygote to the late blastocyst stages. Both groups will be exposed to dTAG-13, but the $Nelfb^{dTAG/+}$ embryos will also have the degradation system engaged since they harbor one $Nelfb^{dTAG}$ allele. Under these conditions embryos developed to late-stage blastocysts at a comparable rate (~80%) to wild-type embryos in the absence of dTAG-13 (Figure 5D and S5C). By contrast, culturing homozygous embryos in dTAG resulted in severe developmental arrest of ~80% of embryos at stages prior to the blastocyst stage (Figure 5C, 5E and 5F). Of note, about 50% were arrested at early cleavage stages, suggesting an early requirement for NELFB in pre-implantation development. To test whether this requirement is specific to the zygote/2-cell stages, we cultured homozygous $Nelfb^{dTAG/dTAG}$ embryos in dTAG from the zygote until the 4-cell stage, or from 4-cell until late blastocyst stage (Figure 5C). An early treatment recapitulated the developmental phenotype of dTAG treatment when present during the entire culture period, while the late treatment had no effect (Figure 5E and S5D). Furthermore, culturing maternal homozygous $mNelfb^{dTAG/dTAG}$; zygotic

heterozygous *Nelfb*$^{dTAG/+}$ embryos (resulting from crossing *Nelfb*$^{dTAG/dTAG}$ females with *Nelfb*$^{+/+}$ males) in dTAG recapitulated the *Nelfb*$^{dTAG/dTAG}$ homozygous embryo defect (Figure 5E and 5F). These experiments suggest that NELFB, and likely maternally provided NELFB, is required for pre-implantation development specifically during the transition from zygote to 2-cell stage, and is dispensable thereafter.

NELFB degradation at the zygote-2-cell stages compromises ZGA

Based on our observation that NELFB is required specifically at the zygote-2-cell stage, we hypothesized that NELFB degradation alters ZGA in mouse embryos. To test this hypothesis, *Nelfb*$^{dTAG/dTAG}$ littermate zygotes were collected and cultured for 30 hours, corresponding to late 2-cell stage, in the presence or absence of dTAG-13. Embryos were then collected from each condition in two replicates, each replicate containing three embryos, for low-input SMART-seq to analyze gene expression (Figure 5A). Samples clustered based on treatment (Figure S6A and S6B). Overall, the expression patterns of 2610 genes were significantly changed (p. adj. > 0.05), with ~53% downregulated (Figure 6 and S6C). Among the differentially expressed genes were ones specific to the 2-cell state and minor ZGA-associated factors, such as *Zscan4e*, *Zscan4d*, and *Dppa4* (Figure 6B)(Hu et al., 2020).

To identify the classes of differentially expressed genes, we used gene clusters present in zygote-to-8-cell stage embryos identified in two previous studies (Abe et al., 2018; Hu et al., 2020). A broad analysis of ~3000 major ZGA-associated genes revealed their overall upregulation in dTAG-13 treated samples (Figure 6C). To further classify the specific identity of upregulated and downregulated genes, we queried the stage-specific clusters (Hu et al. 2020) to which these genes belonged to. Over 50% of downregulated transcripts belonged to genes that peak in the zygote-to-early-2-cell state, coinciding with minor ZGA (Figure 6D). By contrast, over 50% of upregulated genes belonged to major ZGA genes that are initially expressed in late 2-cell stage and increase expression until the 4- and 8-cell stages (Figure 6D). When assessing the overall gene expression levels in each cluster, we find that there is a general increase in clusters representing major ZGA and a decrease in clusters representing minor ZGA (Figure 6E). We obtained similar results when using clusters identified in a different study (Abe et al. 2018, Figure S6D and S6E). Taken together, these results suggest that stage-specific NELFB degradation alters ZGA gene expression, which may result in a compromised minor ZGA and premature major ZGA. These data corroborate previous studies showing that pausing peaks at the zygote-to-early-2-cell stage and decreases at the late 2-cell stage, suggesting that NELFB plays a role in pausing at this stage (Liu et al., 2020).

DISCUSSION

Targeted protein degradation has recently emerged as a method to study protein function in cultured cells (Wu et al., 2020). Here, we successfully adapted one of the promising protein degradation systems, the dTAG system, to the mouse model (Nabet et al., 2018, 2020). Specifically, we show that the dTAG system is efficient and non-toxic across mouse

development and adulthood when administered to embryos in *ex utero* culture or via introduction to pregnant females or adult animals via IP injections.

One of the main advantages of protein degradation is the onset of effect which typically occurs within minutes to hours (Clift et al., 2017; Nabet et al., 2018; Nishimura et al., 2009). This is a major advantage over other RNA/DNA targeting techniques. Our work demonstrates that these rapid dynamics can be achieved in *ex utero* cultured pre-implantation embryos, *in vivo* in post-implantation embryos, and even adult organs with a single IP injection. Notably, near complete degradation of our targeted protein was consistently observed across all these stages, suggesting that the dTAG system is a viable and attractive approach to study acute protein ablation in an inducible manner. Furthermore, the modular nature of the dTAG system enables engaging different ubiquitination pathways with different small molecules which expands the potential tissues and cell lines where they can function (currently CRBN and VHL can be engaged with dTAG-13 and dTAGv-1 respectively)(Nabet et al., 2018, 2020). The efficiency of this system has been demonstrated on a variety of cytosolic, membrane bound, and nuclear proteins in cells suggesting that it is widely applicable irrespective of the cellular localization of the target protein, with the exception of the inner mitochondria membrane (Bensimon et al., 2020; Nabet et al., 2018). One important consideration is that the dynamics of degradation and recovery can vary depending on target protein and tissue, and thus should be validated separately for each case.

The dTAG system can overcome several challenges that are unique to studying protein function in mouse development. One example being transcripts that are maternally deposited prior to zygotic genome activation. Using the dTAG system, one can circumvent the need to use a floxed allele and an oocyte-specific Cre recombinase driver to study essential genes in pre-implantation development. Since tagged alleles can be normally expressed and functional in the absence of dTAG small molecules, it is possible to retrieve 100% of embryos from homozygous crossings that can be induced to be maternal and zygotic deficient of a certain protein. This results in significantly reduced time and resources to obtain maternal/zygotic depleted embryos, and simultaneously a higher yield. Importantly, the rapid inducible and reversable nature of this system enables fine control to define the exact window of necessity of a protein during development and the potential to perform successive depletion-and-recovery cycles. Another challenge that can be overcome with the dTAG system is the inducible depletion of proteins at early post-implantation stages (E5.5 – E7.5). Using CreER systems to study gene function at these stages can be limited by the mosaicism and teratogenicity of tamoxifen (Pimeisl et al., 2013; Ved et al., 2019). Lastly, efficient degradation ensures producing null/knock out-equivalent cellular phenotypes as opposed to deleting certain exons of a gene with ambiguity as to the remaining gene product.

By leveraging the advantages of the dTAG system we gleaned new insights regards the role of NELFB and RNA Pol II pausing during pre-implantation development. *Nelfb* null embryos have been reported to exhibit an early post-implantation lethality, but a role for NELFB in pre-implantation development had not been documented (Amleh et al., 2009). By leveraging the temporal control afforded by the dTAG system with simple mouse genetics and one allele, we uncovered a key role for maternal *Nelfb* in controlling the minor and major ZGA. These observations are in agreement with the reported critical role of *Nelfa* in

the *Drosophila* maternal-to-zygotic (MZT) transition (Wang et al., 2010). Additionally, our data suggest that NELFB regulates expression of minor ZGA genes, and is dispensable for major ZGA, in agreement with the recently reported pausing enrichment prior to major ZGA (Liu et al., 2020). These observations open the door to further studies aimed at determining the molecular mechanisms driving this divergent control of distinct gene sets. Such studies could focus on defining where NELF binds during mammalian ZGA, how it can increase or decrease the transcription output of certain targets during ZGA, and if this effect is specific to ZGA as opposed to prior and later transcription.

Taken together, our data demonstrate that the dTAG system offers unique advantages to other existing perturbation tools and can be applied efficiently *in vivo* across mammalian development.

LIMITATIONS

We present here compelling evidence that the dTAG system is highly efficient and functional in early mammalian development. However, there are few limitations and considerations that should be highlighted. First, as is the case with any other system, efficiency and dynamics of the dTAG system are partially target dependent (Nabet et al., 2018, 2020). Thus, it is necessary to validate degradation of the target protein in cell models before generating mice. Importantly, a fusion protein-tag is required for the system, making it possible that the tag may misfold or impact the protein's function. Thus, it is necessary to validate the function of the tagged protein.

One other *in vivo*-specific limitation is the pharmacokinetics of dTAGv-1 and dTAG-13. Our data suggests that to maintain full degradation of the target protein *in vivo*, injections are required every ~12 hours. Thus, while the system is ideal for short-term studies, it can be cumbersome for long-term studies. This can be potentially circumvented by continuous perfusion systems or development of longer acting *in vivo* dTAG small molecules. While this manuscript was in revision, a pre-print described adapting the AID system to degrade endogenous proteins *in vivo*, thus expanding the available toolbox for *in vivo* protein perturbation (Macdonald et al., 2022).

STAR METHODS

RESOURCE AVAILABILITY

Lead contact—Request for resources and reagents should be directed to and will be fulfilled by the lead contact, Anna-Katerina Hadjantonakis (hadj@mskcc.org)

Materials availability—Plasmids, cell line, and mouse line generated in this study are available upon request from the lead contact.

Data and code availability

- Source data for all figures is available in the supplements, Table S2.
- RNA sequencing data from this work is available in the Gene Expression Omnibus under the accession number GSE185099.

- Any other data reported in this study is available upon request from the lead contact.

EXPERIMENTAL MODEL AND SUBJECT DETAILS

Cell lines—C57BL/6-derived HK3i ES cell line was cultured on 0.1% gelatin (Millipore) coated tissue-culture grade plates in a humidified 37°C incubator with 5% CO_2 (Kiyonari et al., 2010). For routine culture, cells were grown in DMEM (Gibco), supplemented with 2mM L-glutamine (Gibco), 1x MEM non-essential amino acids (Gibco), 1mM sodium pyruvate (Gibco), 100U/ml penicillin and 100μg/ml streptomycin (Gibco), 0.1mM 2-mercaptoethanol (Gibco), 15% KnockOut™ Serum Replacement (Gibco), and 1000U/ml of recombinant leukemia inhibitory factor (LIF). ESCs were maintained on a layer of Mitomycin C inactivated mouse embryonic fibroblasts (MEFs).

Plasmid generation—Two plasmids were generated for this study: (1) Cas9 vector to target the C-terminus of *Nelfb* gene. PX459 vector (addgene #62988) was digested using BbsI-HF (NEB) and single guide RNA targeting *Nelfb* was annealed (Ran et al., 2013), (2) Homology directed repair (HDR) vector containing the insert $FKBP^{F36V}$tag, 2x HA tag, self-cleaving P2A sequence, and Puromycin resistance, flanked by 1 kb *Nelfb* HDR sequences. The insert was obtained from pCRIS-PITCHv2-dTAG-Puro (addgene #91796) (Nabet et al., 2018). The plasmid backbone (pBluescript), *Nelfb* HDR sequences, and the insert were amplified using Q5 polymerase (NEB) and the plasmid was constructed using NEBuilder HiFi DNA assembly (NEB).

Genetic editing—To generate $Nelfb^{dTAG/+}$ mESCs, 3 million cells were transfected with 10ug PX459-Nelfb_sgRNA and 10ug Nelfb_left- $FKBP^{F36V}$- 2xHA- P2A-Puro-Nelfb_right. Cells were transfected using Lonza P3 Primary Cell 4D-Nucleofector™ X 100ul cuvettes (Lonza). Following transfection, cells were plated on a 10 cm dish (Falcon) coated with MEFs. 48 hrs post transfection, correctly targeted cells were selected for using 1.8 ug/ml puromycin (InvivoGen) for 48 hrs. Surviving cells were split 1000 cells/10 cm dish and maintained for 9 days under Puromycin selection. Surviving clones were picked under a stereomicroscope, expanded, and genotyped for the insert.

Mouse strains and husbandry—All animal work was approved by MSKCC Institutional Animal Care and Use Committee (IACUC). Animals were housed in a pathogen-free facility under a 12 hr light cycle. Mouse strains used in this study were $Nelfb^{dTAG}$ and wild-type CD-1/ICR (Charles River). $Nelfb^{dTAG}$ mice were generated by the Mouse Genetics Core at MSKCC. $Nelfb^{dTAG/+}$ ESCs were injected into C57Bl/6 Albino host 8-cell morula. After culturing for 24 hrs in KSOM (Millipore), resulting blastocyst were transferred to pseudo-pregnant females. Only chimeras with ~100% coat color contribution from injected cells were used and mated with CD-1/ICR mice (Chalres River). The resulting colony was outbred to CD-1 three times. Homozygous colony was then established using these mice.

METHOD DETAILS

Cells dTAG treatment—dTAG-13 (Bio-Techne) was reconstituted in DMSO (Sigma) at 5mM. dTAG-13 was diluted in maintenance medium to 500nM and added to cells with medium changes for the specified amounts of time.

Embryo collection—For all experiments, embryos were obtained via natural mating of 6-12 weeks of age females with 7 – 16 weeks of age males. For preimplantation stages, embryos were recovered by flushing the uterine horns (E3.5 – E4.5), the fallopian tubes (E1.5 – E2.5), or dissecting cumulus cells from the fallopian tubes (E0.5). These dissections were carried out in flushing and holding medium (FHM, Millipore) as described (Behringer et al., 2014). To separate zygotes from cumulus cells, cumulus cells-covered embryos were incubated for ~3 mins in 0.3mg/ml Hyaluronidase (Sigma) in FHM.

For post-implantation embryos (E6.5 – E9.5), the uterine horns were retrieved and cut into single decidual swellings in 5% Newborn Calf Serum in DMEM/F12 (Gibco). Embryos were dissected out by removing the uterus wall and decidual tissue. For E6.5-E7.5 embryos, the parietal endoderm was removed carefully with the ectoplacental cone. For E9.5 embryos, the amnion was carefully removed.

Pre-implantation embryo culture—Once recovered, embryos were washed 2 times and cultured in KSOM-AA without phenol red (Millipore). 5-15 Embryos were culture in a 60mm organ culture dish (Falcon) with 700ul KSOM-AA, and 4 ml H20 in the humidifying chamber. Dishes were incubated in a humidified 37°C incubator with 5% CO_2 for up to 96 hrs. For degradation treatments, embryos were incubated with control (KSOM-AA and 0.01% DMSO) or 500nM dTAG-13 (Bio-Techne) in KSOM-AA for the duration of treatment.

Mouse intraperitoneal injections—For intraperitoneal (IP) injections, treatments were formulated in 10% Cremophore EL (Sigma) in sterile PBS+/+. dTAGv-1 (Bio-Techne)/ dTAG-13 was initially reconstituted in DMSO at 1mg/25ul. Prior to injection, 25ul of dTAGv-1/13 or DMSO for vehicle was diluted in 475ul 10% Cremophore EL. Final injection volume was 0.5 ml of 5% DMSO, 10% Cremophore EL in PBS +/+ with or without 1mg dTAGv-1/13 to achieve ~35mg/kg concentration/injection.

Immunofluorescence—For cultured ESCs, cells were plated on u-Slide 8 well (ibidi), washed with PBS+/+ and fixed in 4% PFA (electron microscopy sciences) in PBS+/+ for 10 min at room temperature. Fixed cells were washed two times with PBS+/+, one time with wash buffer; 0.1% Triton X-100 (Sigma) in PBS+/+, then permeabilized in 0.5% Triton X-100 (Sigma) in PBS+/+ for 10 min. Cells were then blocked with 3% Donkey Serum (Sigma) and 1% BSA (Sigma) for 1 hr at room temperature. Cells were then incubated with mouse anti-HA (abcam, 1:500) in blocking buffer at 4°C over night. Cells were then washed three times in wash buffer, and incubated with donkey anti-mouse Alexa Fluor™ 488 (Invitrogen, 1:500) for 1 hr at room temperature. Cells were then washed three time wish wash buffer, the last containing 5μg/ml Hoechst 33342 (Invitrogen), then imaged.

For E3.5-E4.5 pre-implantation embryos, the zona pellucida was removed by incubation in acid Tyrode's solution (Sigma) at 37°C for 2 min. Embryos were subsequently washed briefly in PBS+/+ before fixation in 4% PFA for 10 mins at room temperature. Fixed embryos were washed in 0.1% Triton X-100 in PBS+/+ (PBX)for 5 min, permeabilized in 0.5% Triton X-100 (Sigma) in PBS+/+ for 5 min, washed again for 5 min in PBX, and blocked in 2% horse serum (Sigma) in PBS+/+ for 1 hr at room temperature. Embryos were incubated in primary antibodies diluted in blocking solution over night at 4°C. Embryos were then washed three times for 5 min each in PBX and blocked again for 1 hr at room temperature prior to incubation with secondary antibodies. Secondary antibodies diluted in blocking solution were applied for 1 hr at 4°C. Embryos were then washed twice for 5 min each in PBX and incubated with 5ug/ml Hoechst 33342 (Invitrogen) in PBS for 5 min or until mounting for imaging. The following primary antibodies were used: goat anti-GATA6 (R&D Systems, 1:100), mouse anti-CDX2 (BioGenex, 1:200), rabbit anti-NANOG (CosmoBio, 1:500), mouse anti-HA (abcam, 1:500), rabbit anti-HA (Cell Signaling, 1:200). Secondary Alexa Fluor-conjugated antibodies (Invitrogen) were used at a dilution of 1:500. DNA was visualized using Hoechst 33342.

For E0.5-E1.5 embryos, the staining was identical to E3.5-E4.5 embryos except for fixation for 50 min at room temperature in 4% PFA, permeabilization for 30 min at room temperature, and blocking solution is 1% BSA in PBS+/+.

For E6.5 and E 7.5, Embryos were washed briefly in PBS+/+ before fixation in 4% PFA for 20 mins at room temperature. Fixed embryos were washed in 0.1% Triton X-100 in PBS+/+ (PBX) for 5 min, permeabilized in 0.5% Triton X-100 (Sigma) in PBS+/+ for 20 min, washed again for 5 min in PBX, and blocked in 3% horse serum (Sigma) in PBX for 1 hr at room temperature. Embryos were incubated in primary antibodies diluted in blocking solution over night at 4°C. Embryos were then washed three times for 10 min each in PBX and blocked again for 1 hr at room temperature prior to incubation with secondary antibodies. Secondary antibodies diluted in blocking solution were applied over night at 4°C. Embryos were then washed three times for 5 min each in PBX and incubated with 5ug/ml Hoechst 33342 (Invitrogen) in PBX for 1 hr or until mounting for imaging.

For E9.5, embryos were fixed in 4% PFA for 40 mins at room temperature. Fixed embryos were washed in 0.1% Triton X-100 in PBS+/+ (PBX) for 15 min, permeabilized in 0.5% Triton X-100 (Sigma) in PBS+/+ for 1 hr, then blocked in 5% horse serum (Sigma) in PBX for 2 hrs at room temperature. Embryos were incubated in primary antibodies diluted in blocking solution over night at 4°C. Embryos were then washed in PBX three times for 30 mins each and blocked again for 2 hrs prior to incubation in secondary antibodies and Hoechst over night at 4°C. Embryos were subsequently washed three times for 30 mins each in PBX. Embryos were mounted in Ce3D clearing solution 4 hrs before imaging (Li et al., 2019).

Confocal image data acquisition from fixed embryos—Fixed immunostained samples were imaged on a Zeiss LSM880 laser scanning confocal microscope. Pre-implantation embryos were mounted in microdroplets of 5μg/ml Hoechst 33342 in PBS+/+ on glass-bottomed dished (MatTek) coated with mineral oil (Sigma). Embryos were imaged

along the entire z-axis with 1μm step using an oil-immersion Zeiss EC Plan-Neofluar 40x/NA 1.3 with a 0.17mm working distance. For post-implantation embryos, a similar setup was used but with an air Plan-Apochromat 20x/NA 0.75 objective.

Low magnification pooled embryo images and E9.5 full embryos were imaged on a Zeiss Axio Zoom.Vie using a PlanNeoFluar Z 1x/0.25 FWD 56mm objective. Pseudo-stacking (Zeiss ZEN Blue) was used for E9.5 images.

Western blotting—For cells, 350μl of lysis buffer; 1x Cell Lysis Buffer (Cell Signaling) with 1mM PMSF (Cell Signaling) and cOmplete™ Ultra protease inhibitor (Sigma), was added to a 90% confluent 6-well dish (Falcone) after washing with PBS−/−. Cells were incubated with lysis buffer for 5 min on ice, then scraped and collected. Samples were sonicated for 15 seconds to complete lysis at, then spun down at 12,000x g for 10 min at 4°C. The supernatant was collected, and protein concentration measured using Pierce™ BCA Protein Assay Kit (Thermo). 20ug of protein was mixed with Blue Loading Buffer (Cell Signaling) and 40mM DTT (Cell signaling). Samples were boiled at 95°C for 5 min for denaturation. For tissue samples, similar protocol was followed, except that 100mg of tissue was homogenized in 1ml lysis using a Dounce homogenizer for 30 mins on ice.

Samples were run on a BioRad PROTEAN system and transferred using Trans-Blot Semi-Dry Transfer Cell (BioRad) to a nitrocellulose membrane (Cell Signaling) following manufacturer's instructions and reagents. Membranes were then washed briefly with ddH2O and stained with Ponceau S (Sigma) for 1 min to check for transfer quality, and as a loading control. Membranes were then washed three times with TBST; 0.1% Tween 20 (Fisher) in TBS. Membranes were blocked with 4% BSA in TBST for 1 hr at room temperature and subsequently incubated with primary antibodies diluted in blocking buffer at 4°C over night. They were then washed three times with TBST, then incubated with secondary antibodies in blocking buffer for 1 hr. Washed three times with TBST, incubated with ECL reagent SignalFire™ for 1-2 min and imaged using a ChemiDoc (BioRad). The following antibodies were used: rabbit anti-HA (Cell Signaling, 1:1000), mouse anti-b-Actin (Cell Signaling, 1:3000), anti-rabbit IgG, HRP-linked (Cell signaling, 1:2000), anti-mouse IgG, HRP-linked (Cell signaling, 1:2000).

RT-qPCR—RNA was extracted from samples using TRIzol (Thermo) following the manufacturer's instructions, 1μg of RNA was used to generate cDNA using the QuantiTect reverse transcription kit (Qiagen). qPCR reaction was performed using PowerUp SYBR green mastermix (thermo) and a BioRad CFX96. Used primers are available in (Table S1).

Stereotaxic intracranial injections—Four-month-old female *Nelfb*$^{dTAG/dTAG}$ mice were anesthetized with 2.5% isoflurane and 80% O_2 and head-fixed in a stereotaxic frame (David Kopf Instruments, Tujunga, CA) equipped with digital manipulator arms (Stoelting Co, Wood Dale, IL). A nose cone was used to deliver isoflurane to maintain anesthesia. Mice were given subcutaneous injection of meloxicam (2mg/kg) and 0.1 mL of 0.25% Marcaine around the incision site. After exposing the skill, craniotomies were made with an electric drill (Stoelting CO, Wood Dale, IL) with a ball bur attached. A Neuros 7000 series 1 μL Hamilton syringe with a 33-gauge needle (Hamilton Company, Reno, NV) connected to

a remote automated microinfusion pump (KD Scientific, Holliston, MA) was used for drug delivery at a rate of 100 nL/min into the left somatosensory cortex (A/P: 0 mm, M/L: 2.50 mm, D/V −1.50 mm). 200 nL of 1mM dTAG-1 or dTAG-13 was infused into each animal. Following infusion, the needle was left in place for 5 min and then slowly manually retracted to allow for diffusion and prevent backflow of the drug. Mice were monitored while on a heat pad for at least 30 min post-surgery before being returned to their home-cage.

Brain tissue preparation—Mice were euthanized 2 hrs after the infusion of dTAG-1 or dTAG-13 anesthetized mice were perfused transcardially with room temperature PBS with 0.02mg/mL heparin (Heparin sodium salt 50KU) and then ice-cold 4% paraformaldehyde. Brains were dissected and post-fixed in the same fixative overnight at 4°C and cryopreserved in 30% sucrose in PBS for 2 days at 4°C. Brains were embedded in Tissue-Tek OCT compound (Sakura Finetek). Serial cryosectioning was performed at 50μm using a cryostat (Leica) and collected in 0.01M phosphate buffer with 0.02% sodium azide and kept at 4°C until further processing.

Brain tissue immunofluorescence—For cryosectioned adult brain tissue, free-floating sections were first washed three times in PBS for 5 min each. Sections were then incubated in 10% normal donkey serum (NDS) in 0.5% Triton-X100 in PBS (PBX) for 1 hr before incubating in primary antibody solution made in 2% NDS in 0.4% PBX for 48 hrs at 4°C. Sections were washed with PBS three times for 5 min each and incubated in secondary antibody solution in 2% NDS in 0.4% PBX (1:500) for 2 hrs at RT. Following secondary antibody staining, slides were incubated in Hoechst 33258 (1:1000 in PBS) for 10 min and washed with PBS three times for 5 min each. Sections were mounted on glass slides and once fully dried were coverslipped with Fluoro-Gel (Electron Microscopy Sciences) and stored at 4°C until imaging. Whole brain section images were obtained using NanoZoomer Digital Pathology (Hamamatsu Photonics) and 20x objective. Higher power confocal images for quantification purposes were acquired via Zeiss LSM880. Region immediately outside of the injection area was used as control. Three intensity measurements were taken from three consecutive thalamic-level sections per biological replicate/mouse using Fiji. The regions are circles on high magnification images with several nuclei included. HA signal was normalized to Hoechst, then control regions across sections.

RNA transcriptomics—Sequencing was done by the MSKCC Integrated Genomics Operations (IGO). SMART-seq v4 Ultra Low Input pipeline was used (Clonetech/Takara). Three 2-cell stage embryos were added to 5μl of 10x Lysis Buffer (Takara) and RNase inhibitor (Takara) per manufacturer's instructions. Samples were immediately frozen on dry ice and stored at −80 until cDNA amplification, library prep, and sequencing using NovaSeq 6000.

Quantification and statistical analyses

Image processing and quantification: For Pre-implantation embryos, semi-automated 3D nuclear segmentation for cell counting and quantification of fluorescence intensity was carried out using MINS, a MATLAB-based algorithm (http://katlab-tools.org/) (Lou et al., 2014). The same imaging parameters were used for all experiments consisting of

the same primary and secondary antibody combinations to minimize quantitative variance due to image acquisition. The MINS output was checked for over- or under-segmentation and tables were corrected manually using Image J (NIH, https://imagej.nih.gov/ij/). Under-segmented nuclei (two or more nuclei detected as one, or nuclei that were not detected) were assigned fluorescence intensity values that were directly measured using ImageJ (NIH). To correct fluorescence decay along the Z-axis, we used a linear regression method to calculate the global average of the regression coefficients in the HA channel (Saiz et al., 2016).This slope was then used to adjust the logarithm values of HA fluorescence intensity for each nucleus. Trophectoderm (TE) vs. inner cell mass (ICM) cell assignment was achieved by a threshold for CDX2 which is present exclusively in TE. To avoid batch variability, directly compared embryos were stained and imaged in the same session.

For post-implantation embryos, fluorescence intensities were acquired manually per embryo by measuring HA and Hoechst in ~10 nuclei. HA signal was normalized to Hoechst per embryo, and all measurements were compared only to similar age embryos that were stained and imaged in the same session, except for E7.5 time series which was done over two sessions due to embryos number. All embryos were stained, imaged, and processed using the same parameters, and intensity quantifications were measured at the same Z-depth across all embryos to omit the need for Z-fluorescence decay normalization.

Statistical analyses: All statistical tests of immunofluorescence data were carried out in PRISM 9 (GraphPad). Statical significance was established using a two-tailed student t-test with p-value threshold of 0.05. The p-value range for each experiment is indicated in the figure legend.

For sequencing data, analysis of differentially expressed genes was done in R using the DEseq2 method (Love et al., 2014).

PREPARATION OF FIGURES

Figures which included panels of image data, blots, and plots, as well as illustrations, were assembled using Adobe Creative Cloud (https://www.adobe.com/creativecloud.html) using Illustrator and Photoshop applications, with additional illustrations obtained from BioRender (https://biorender.com/).

Supplementary Material

Refer to Web version on PubMed Central for supplementary material.

ACKNOWLEDGEMENTS

We thank MSK's Mouse Genetics Core Facility for assistance in generating *Nelfb*^{dTAG} mice and the Integrated Genomics Operation and Bioinformatics Core Facility for assistance in sequencing and sequence data analysis. We are grateful to members of the Hadjantonakis lab for stimulating discussion and critical feedback. AA is supported by a MSTP training grant from the NIH (T32GM007739) awarded to the Weill Cornell/Rockefeller/Sloan Kettering Tri-Institutional MD-PhD Program and NIH F30HD103398. Work in AKH's lab is supported by the NIH (R01HD094868, R01DK127821, R01HD086478, and P30CA008748). Work in ALJ's lab is supported by NIH grants (R01NS092096, R37MH085726 and a NCI Cancer Center Support Grant P30CA008748-48). ASL in ALJ's lab is supported by Weill Cornell Medicine Clinical & Translational Science Center Predoctoral Training Award (TL1TR002386) from National Center for Advancing Translational Sciences.

REFERENCES

Abe K-I, Funaya S, Tsukioka D, Kawamura M, Suzuki Y, Suzuki MG, Schultz RM, and Aoki F (2018). Minor zygotic gene activation is essential for mouse preimplantation development. Proc. Natl. Acad. Sci. U. S. A 115, E6780–E6788. [PubMed: 29967139]

Abuhashem A, Garg V, and Hadjantonakis A-K (2022). RNA polymerase II pausing in development: orchestrating transcription. Open Biol. 12, 210220. [PubMed: 34982944]

Adelman K, and Lis JT (2012). Promoter-proximal pausing of RNA polymerase II: emerging roles in metazoans. Nat Rev. Genet 13, 720–731. [PubMed: 22986266]

Amleh A, Nair SJ, Sun J, Sutherland A, Hasty P, and Li R (2009). Mouse cofactor of BRCA1 (Cobra1) is required for early embryogenesis. PLoS One 4, 2–9.

Bardot ES, and Hadjantonakis A-K (2020). Mouse gastrulation: Coordination of tissue patterning, specification and diversification of cell fate. Mech. Dev 163, 103617. [PubMed: 32473204]

Behringer R, Gertsenstein M, Nagy KV, and Nagy A (2014). Manipulating the Mouse Embryo: A Laboratory Manual (Cold Spring Harbor Laboratory Press).

Bensimon A, Pizzagalli MD, Kartnig F, Dvorak V, Essletzbichler P, Winter GE, and Superti-Furga G (2020). Targeted Degradation of SLC Transporters Reveals Amenability of Multi-Pass Transmembrane Proteins to Ligand-Induced Proteolysis. Cell Chem. Biol 27, 728–739.e9. [PubMed: 32386596]

Chamberlain PP, D'Agostino LA, Ellis JM, Hansen JD, Matyskiela ME, McDonald JJ, Riggs JR, and Hamann LG (2019). Evolution of Cereblon-Mediated Protein Degradation as a Therapeutic Modality. ACS Med. Chem. Lett 10, 1592–1602. [PubMed: 31857833]

Clift D, McEwan WA, Labzin LI, Konieczny V, Mogessie B, James LC, and Schuh M (2017). A Method for the Acute and Rapid Degradation of Endogenous Proteins. Cell 171, 1692–1706.e18. [PubMed: 29153837]

Core L, and Adelman K (2019). Promoter-proximal pausing of RNA polymerase II: a nexus of gene regulation. Genes Dev. 33, 960–982. [PubMed: 31123063]

Hu Z, Tan DEK, Chia G, Tan H, Leong HF, Chen BJ, Lau MS, Tan KYS, Bi X, Yang D, et al. (2020). Maternal factor NELFA drives a 2C-like state in mouse embryonic stem cells. Nat. Cell Biol 22, 175–186. [PubMed: 31932739]

Jaeger MG, and Winter GE (2021). Fast-acting chemical tools to delineate causality in transcriptional control. Mol. Cell 81, 1617–1630. [PubMed: 33689749]

Kiyonari H, Kaneko M, Abe S, and Aizawa S (2010). Three inhibitors of FGF receptor, ERK, and GSK3 establishes germline-competent embryonic stem cells of C57BL/6N mouse strain with high efficiency and stability. Genesis 48, 317–327. [PubMed: 20162675]

Kwak H, and Lis JT (2013). Control of Transcriptional Elongation. Annu. Rev. Genet 47, 483–508. [PubMed: 24050178]

Li W, Germain RN, and Gerner MY (2019). High-dimensional cell-level analysis of tissues with Ce3D multiplex volume imaging. Nat. Protoc 14, 1708–1733. [PubMed: 31028373]

Liu B, Xu Q, Wang Q, Feng S, Lai F, Wang P, Zheng F, Xiang Y, Wu J, Nie J, et al. (2020). The landscape of RNA Pol II binding reveals a stepwise transition during ZGA. Nature 587, 139–144. [PubMed: 33116310]

Lou X, Kang M, Xenopoulos P, Munoz-Descalzo S, and Hadjantonakis A-K (2014). A rapid and efficient 2D/3D nuclear segmentation method for analysis of early mouse embryo and stem cell image data. Stem Cell Reports 2, 382–397. [PubMed: 24672759]

Love MI, Huber W, and Anders S (2014). Moderated estimation of fold change and dispersion for RNA-seq data with DESeq2. Genome Biol. 15, 550. [PubMed: 25516281]

Macdonald L, Taylor G, Brisbane J, Christodoulou E, Scott L, Von Kriegsheim A, Rossant J, Gu B, and Wood A (2022). Rapid and specific degradation of endogenous proteins in mouse models using auxin-inducible degrons. BioRxiv 2022.01.13.476100.

Nabet B, Roberts JM, Buckley DL, Paulk J, Dastjerdi S, Yang A, Leggett AL, Erb MA, Lawlor MA, Souza A, et al. (2018). The dTAG system for immediate and target-specific protein degradation. Nat Chem. Biol 14, 431–441. [PubMed: 29581585]

Nabet B, Ferguson FM, Seong BKA, Kuljanin M, Leggett AL, Mohardt ML, Robichaud A, Conway AS, Buckley DL, Mancias JD, et al. (2020). Rapid and direct control of target protein levels with VHL-recruiting dTAG molecules. Nat Commun. 11, 4687. [PubMed: 32948771]

Nishimura K, Fukagawa T, Takisawa H, Kakimoto T, and Kanemaki M (2009). An auxin-based degron system for the rapid depletion of proteins in nonplant cells. Nat Methods 6, 917–922. [PubMed: 19915560]

Nishimura K, Yamada R, Hagihara S, Iwasaki R, Uchida N, Kamura T, Takahashi K, Torii KU, and Fukagawa T (2020). A super-sensitive auxin-inducible degron system with an engineered auxin-TIR1 pair. Nucleic Acids Res. 48, e108. [PubMed: 32941625]

Nowotschin S, Setty M, Kuo Y-Y, Liu V, Garg V, Sharma R, Simon CS, Saiz N, Gardner R, Boutet SC, et al. (2019). The emergent landscape of the mouse gut endoderm at single-cell resolution. Nature 569, 361–367. [PubMed: 30959515]

Pickar-Oliver A, and Gersbach CA (2019). The next generation of CRISPR-Cas technologies and applications. Nat. Rev. Mol. Cell Biol 20, 490–507. [PubMed: 31147612]

Pijuan-Sala B, Griffiths JA, Guibentif C, Hiscock TW, Jawaid W, Calero-Nieto FJ, Mulas C, Ibarra-Soria X, Tyser RCV, Ho DLL, et al. (2019). A single-cell molecular map of mouse gastrulation and early organogenesis. Nature 566, 490–495. [PubMed: 30787436]

Piliszek A, Kwon GS, and Hadjantonakis A-K (2011). Ex utero culture and live imaging of mouse embryos. Methods Mol. Biol 770, 243–257. [PubMed: 21805267]

Pimeisl I-M, Tanriver Y, Daza RA, Vauti F, Hevner RF, Arnold H-H, and Arnold SJ (2013). Generation and characterization of a tamoxifen-inducible Eomes(CreER) mouse line. Genesis 51, 725–733. [PubMed: 23897762]

Poueymirou WT, Auerbach W, Frendewey D, Hickey JF, Escaravage JM, Esau L, Doré AT, Stevens S, Adams NC, Dominguez MG, et al. (2007). F0 generation mice fully derived from gene-targeted embryonic stem cells allowing immediate phenotypic analyses. Nat. Biotechnol 25, 91–99. [PubMed: 17187059]

Rahl PB, Lin CY, Seila AC, Flynn RA, McCuine S, Burge CB, Sharp PA, and Young RA (2010). c-Myc regulates transcriptional pause release. Cell 141, 432–445. [PubMed: 20434984]

Ran FA, Hsu PD, Wright J, Agarwala V, Scott DA, and Zhang F (2013). Genome engineering using the CRISPR-Cas9 system. Nat Protoc. 8, 2281–2308. [PubMed: 24157548]

Saiz N, Plusa B, and Hadjantonakis A-K (2015). Single cells get together: High-resolution approaches to study the dynamics of early mouse development Semin. Cell Dev. Biol 47-48, 92–100.

Saiz N, Williams KM, Seshan VE, and Hadjantonakis A-K (2016). Asynchronous fate decisions by single cells collectively ensure consistent lineage composition in the mouse blastocyst Nat. Commun 7, 13463. [PubMed: 27857135]

Savery D, Maniou E, Culshaw LH, Greene NDE, Copp AJ, and Galea GL (2020). Refinement of inducible gene deletion in embryos of pregnant mice. Birth Defects Res. 112, 196–204. [PubMed: 31793758]

Schindelin J, Arganda-Carreras I, Frise E, Kaynig V, Longair M, Pietzsch T, Preibisch S, Rueden C, Saalfeld S, Schmid B, et al. (2012). Fiji: an open-source platform for biological-image analysis. Nat. Methods 9, 676–682. [PubMed: 22743772]

Schrode N, Xenopoulos P, Piliszek A, Frankenberg S, Plusa B, and Hadjantonakis A-K (2013). Anatomy of a blastocyst: Cell behaviors driving cell fate choice and morphogenesis in the early mouse embryo. Genesis 51, 219–233. [PubMed: 23349011]

Smits AH, Ziebell F, Joberty G, Zinn N, Mueller WF, Clauder-Münster S, Eberhard D, Fälth Savitski M, Grandi P, Jakob P, et al. (2019). Biological plasticity rescues target activity in CRISPR knock outs. Nat. Methods 16, 1087–1093. [PubMed: 31659326]

Sun Q-Y, Liu K, and Kikuchi K (2008). Oocyte-specific knockout: a novel in vivo approach for studying gene functions during folliculogenesis, oocyte maturation, fertilization, and embryogenesis. Biol. Reprod 79, 1014–1020. [PubMed: 18753607]

Tadros W, and Lipshitz HD (2009). The maternal-to-zygotic transition: a play in two acts. Development 136, 3033–3042. [PubMed: 19700615]

Ved N, Curran A, Ashcroft FM, and Sparrow DB (2019). Tamoxifen administration in pregnant mice can be deleterious to both mother and embryo. Lab. Anim 53, 630–633. [PubMed: 31248325]

Verma R, Mohl D, and Deshaies RJ (2020). Harnessing the Power of Proteolysis for Targeted Protein Inactivation. Mol. Cell 77, 446–460. [PubMed: 32004468]

Vos SM, Farnung L, Urlaub H, and Cramer P (2018a). Structure of paused transcription complex Pol II–DSIF–NELF. Nature.

Vos SM, Farnung L, Urlaub H, and Cramer P (2018b). Structure of paused transcription complex Pol II–DSIF–NELF. Nature 560, 601–606. [PubMed: 30135580]

Vos SM, Farnung L, Boehning M, Wigge C, Linden A, Urlaub H, and Cramer P (2018c). Structure of activated transcription complex Pol II-DSIF-PAF-SPT6. Nature 560, 607–612. [PubMed: 30135578]

Wang X, Hang S, Prazak L, and Gergen JP (2010). NELF Potentiates Gene Transcription in the Drosophila Embryo. PLoS One 5, e11498. [PubMed: 20634899]

Williams LH, Fromm G, Gokey NG, Henriques T, Muse GW, Burkholder A, Fargo DC, Hu G, and Adelman K (2015). Pausing of RNA Polymerase II Regulates Mammalian Developmental Potential through Control of Signaling Networks. Mol. Cell 58, 311–322. [PubMed: 25773599]

Wu T, Yoon H, Xiong Y, Dixon-Clarke SE, Nowak RP, and Fischer ES (2020). Targeted protein degradation as a powerful research tool in basic biology and drug target discovery. Nat. Struct. Mol. Biol 27, 605–614. [PubMed: 32541897]

Yamaguchi Y, Takagi T, Wada T, Yano K, Furuya A, Sugimoto S, Hasegawa J, and Handa H (1999). NELF, a multisubunit complex containing RD, cooperates with DSIF to repress RNA polymerase II elongation. Cell 97, 41–51. [PubMed: 10199401]

Yesbolatova A, Saito Y, Kitamoto N, Makino-Itou H, Ajima R, Nakano R, Nakaoka H, Fukui K, Gamo K, Tominari Y, et al. (2020). The auxin-inducible degron 2 technology provides sharp degradation control in yeast, mammalian cells, and mice. Nat. Commun 11, 5701. [PubMed: 33177522]

HIGHLIGHTS

- A mouse model to evaluate kinetics and efficacy of the dTAG degron system *in vivo*
- Acute and efficient protein degradation during *in utero* embryo development
- Fine temporal induction and reversibility across embryonic stages and adult tissues
- Acute stage-specific depletion reveals a role for NELFB during mouse ZGA

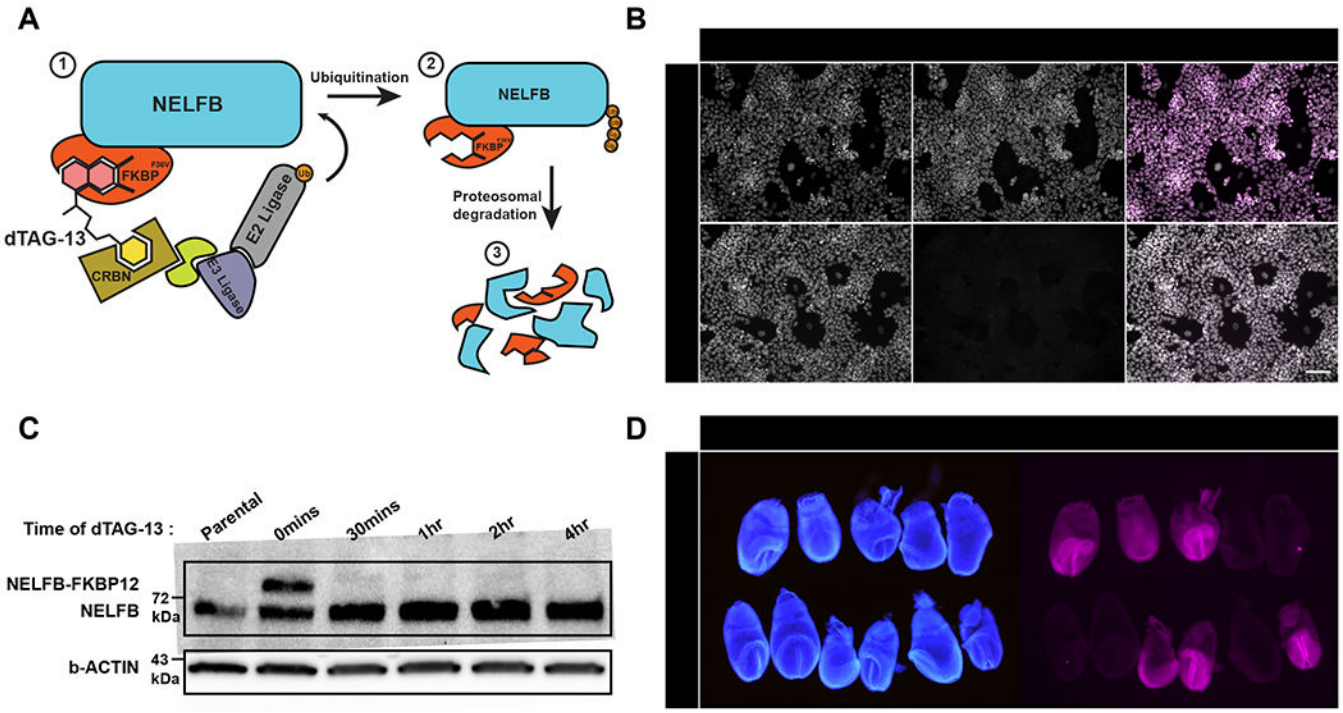

Figure 1.

Generation of *Nelfb*^{dTAG} mouse model to study the dTAG system *in vivo*.

(A) Schematic illustration of the proteasomal degradation in the dTAG system. The numbers represent the sequence of events from recognition of tag to degradation.

(B) Immunofluorescence of targeted mESCs showing nuclear localized HA signal corresponding to NELFB +/− 500nM dTAG-13 treatment for 30 mins. Nuclei labeled with Hoechst. Scale bar, 70μm.

(C) Western blot of targeted mES cells' whole cell lysates +/− dTAG-13 treatment for indicated time intervals. Anti-NELFB antibody was used. 20ug of protein loaded/lane.

(D) Immunofluorescence of a single E7.5 litter from a heterozygous *Nelfb*$^{dTAG/+}$ male and wild-type *Nelfb*$^{+/+}$ female showing germline transmission of the targeted allele. Nuclei labeled with Hoechst. Scale bar, 500μm.

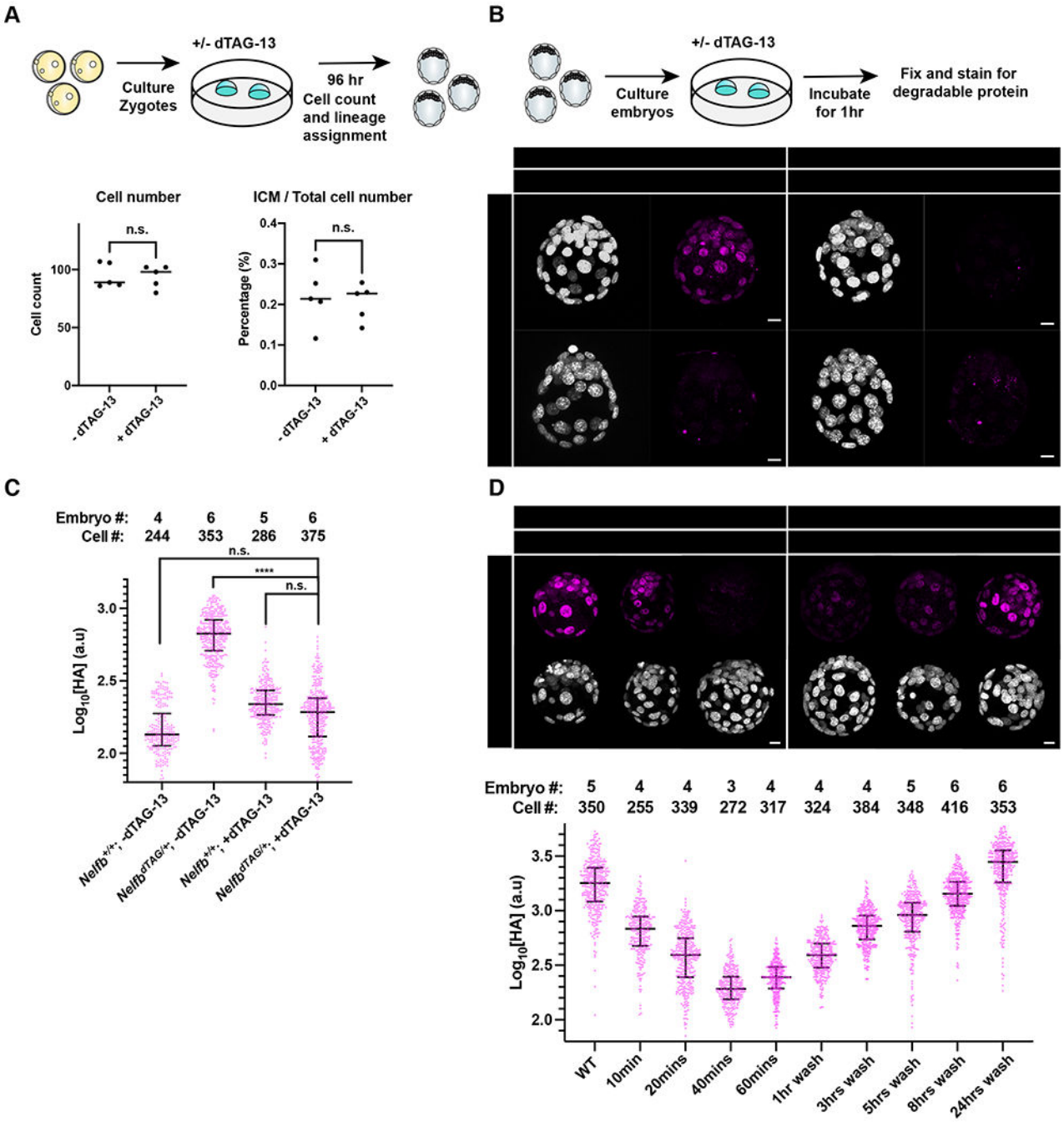

Figure 2.

Establishing safety and efficiency of the dTAG system in pre-implantation stages.

(A) (Top) Schematic representation of experimental design to test dTAG-13 safety in pre-implantation culture from zygote to blastocyst stages. (Bottom) Dot plots showing total cell counts (left) or percent ICM cells (right). Cell counts were determined following Hoechst staining and nuclei counting. ICM cells were identified via NANOG/GATA6 staining. Individual dots represent single embryos. Bars represent group means.

(B) (Top) Schematic representation of experimental design to determine efficacy of tagged protein degradation. E3.5 blastocysts were cultured +/− 500nM dTAG-13 for 1hr prior to fixation and immunostaining. (Bottom) Immunofluorescence of HA to determine degradation of tagged protein. Nuclei labeled with Hoechst. Total cell count per embryo is shown in the top left corner. Scale bar, 10μm.

(C) Quantification of mean HA signal intensity per nucleus. Wild type embryos used to show background fluorescence with staining.

(D) (Top) E3.5 immunofluorescence of HA to determine degradation of tagged protein following several indicated incubation periods or following degradation and recovery in dTAG-13-free medium. Nuclei labeled with Hoechst. (Bottom) Quantification of mean HA signal intensity per nucleus. Scale bar, 10μm.

For all experiments, maximum intensity projection (MIP) is shown in images. Plots show each data point with group mean and interquartile range. Student t-test was used to determine significance. Statistical significance is classified based on p-value as: n.s. > 0.05, * < 0.05, ** < 0.01, *** < 0.001, **** < 0.0001.

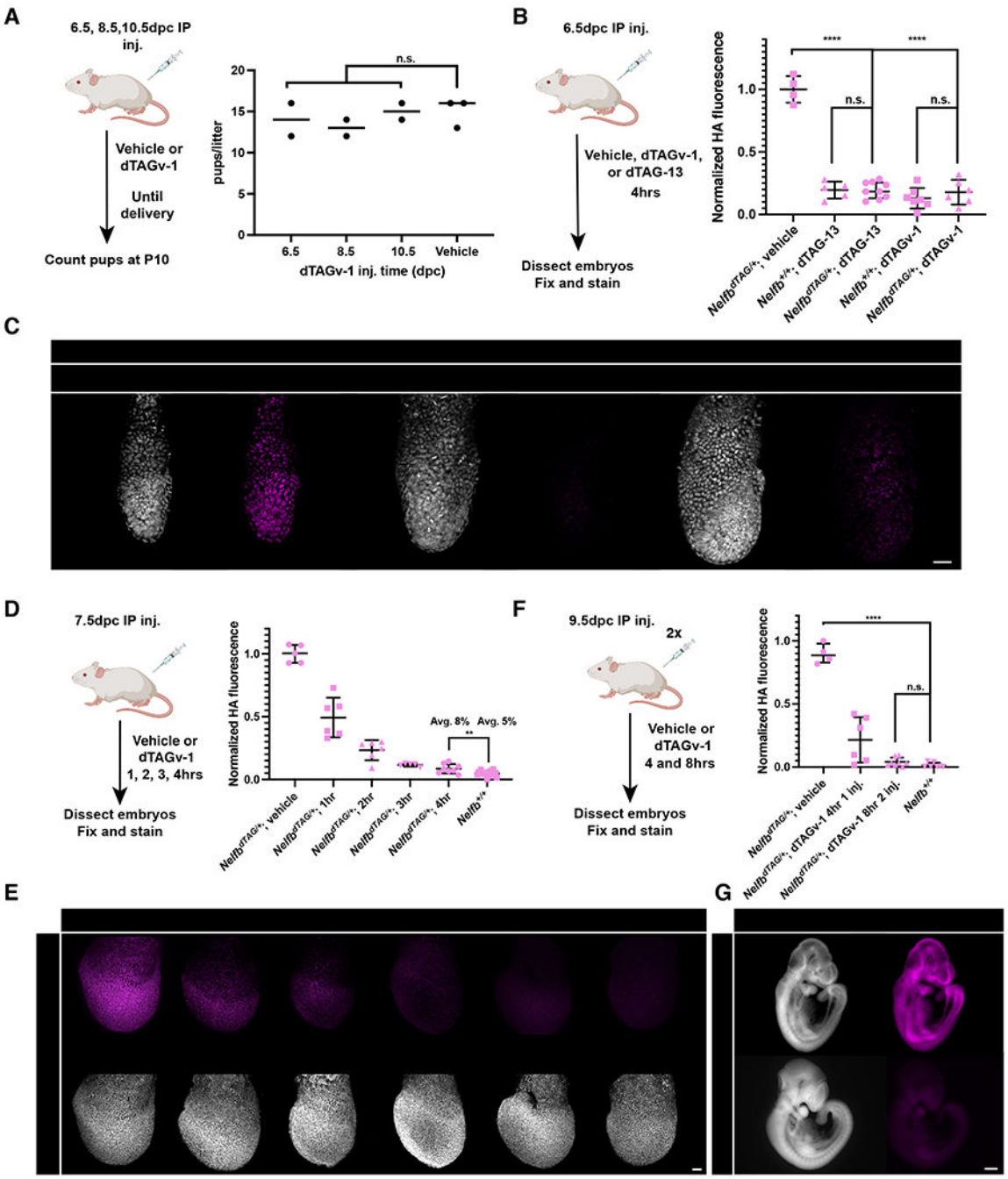

Figure 3.

Establishing safety and efficiency of the dTAG system in post-implantation stages.

(A) (Left) Schematic of testing dTAGv-1 safety in post-implantation development *in vivo*. Wild type pregnant females were given IP injection of 35mg kg^{-1} dTAGv-1 at 6.5, 8.5, 10.5 days post conception (dpc). (Right) Resulting healthy pups at term were counted.

(B) Quantification of HA mean signal intensity in E6.5 embryos 4hrs after heterozygous *Nelfb*$^{dTAG/+}$ pregnant females received dTAGv-1 or dTAG-13 injection. Each dot represents an embryo. HA signal was normalized to Hoechst, then vehicle injected litters.

(C) Immunofluorescence images of E6.5 embryos retrieved 4hrs after pregnant females received IP injection of dTAGv-1 or dTAG-13. Nuclei are labeled by Hoechst. Scale bars, 50μm.

(D) Quantification of HA mean signal intensity in E7.5 embryos 1,2,3, or 4hrs after heterozygous *Nelfb*$^{dTAG/+}$ pregnant females received dTAGv-1 injection. Each dot represents an embryo. HA signal was normalized to Hoechst, then vehicle injected litters.

(E) Immunofluorescence images of E7.5 embryos retrieved 1,2,3 and 4hrs after pregnant females received IP injection of dTAGv-1. Nuclei are labeled by Hoechst. Scale bars, 50μm.

(F) Quantification of HA mean signal intensity in E9.5 embryos 4 and 8hrs after heterozygous *Nelfb*$^{dTAG/+}$ pregnant females received one dTAGv-1 injection, or two separated by 2hrs and followed for 6hrs after the second for a total 8hrs from first injection. Each dot represents an embryo. HA signal was normalized to Hoechst, then vehicle injected litters.

(G) Immunofluorescence images of E9.5 embryos retrieved 8hrs after pregnant females received two IP injections of dTAGv-1. Nuclei are labeled by Hoechst. Scale bars, 500μm.

For all experiments, maximum intensity projection (MIP) is shown in images. Plots show each data point with group mean and interquartile range. Student t-test was used to determine significance. Statistical significance is classified based on p-value as: n.s. > 0.05, * < 0.05, ** < 0.01, *** < 0.001, **** < 0.0001.

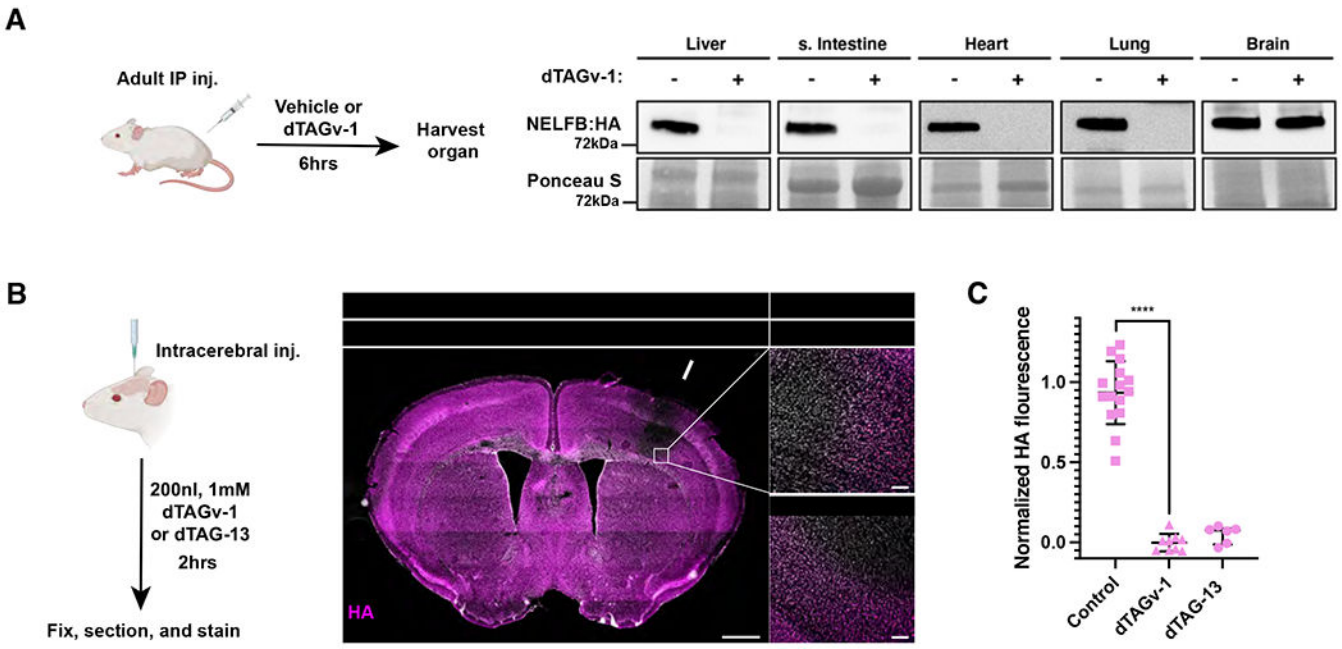

Figure 4.

Establishing efficiency of the dTAG system in adult mouse tissues.

(A) Western blot of HA signal levels in lysates from several organs 6hrs after IP injection of dTAGv-1.

(B) (Left) Schematic of stereotaxic intracerebral injection of dTAGv-1 and dTAG-13 into the somatosensory cortex to determine the dTAG system degradation efficiency in brain tissue. (Middle) Immunofluorescence of stitched images of a whole brain coronal section post injection of dTAG-13 at the level of the somatosensory cortex/striatum. Arrow points to the injection site. Nuclei are labeled by Hoechst. Scale bars, 1mm. (Right) Zoom-in image of the injection area border showing loss of HA in nuclei in brains injected with dTAGv-1 or dTAG-13. Scale bars, 100 μm.

(C) Quantification of HA mean signal intensity in adult mouse brain tissue 2hrs after homozygous *Nelfb*$^{dTAG/dTAG}$ females received dTAGv-1 or dTAG-13 injection. Region immediately outside of the injection area was used as control. Three measurements were taken from three sections per biological replicate/mouse. The regions are squares on high magnification images with several nuclei included. HA signal was normalized to Hoechst, then control regions. Student t-test was used to determine significance and p-value **** < 0.0001.

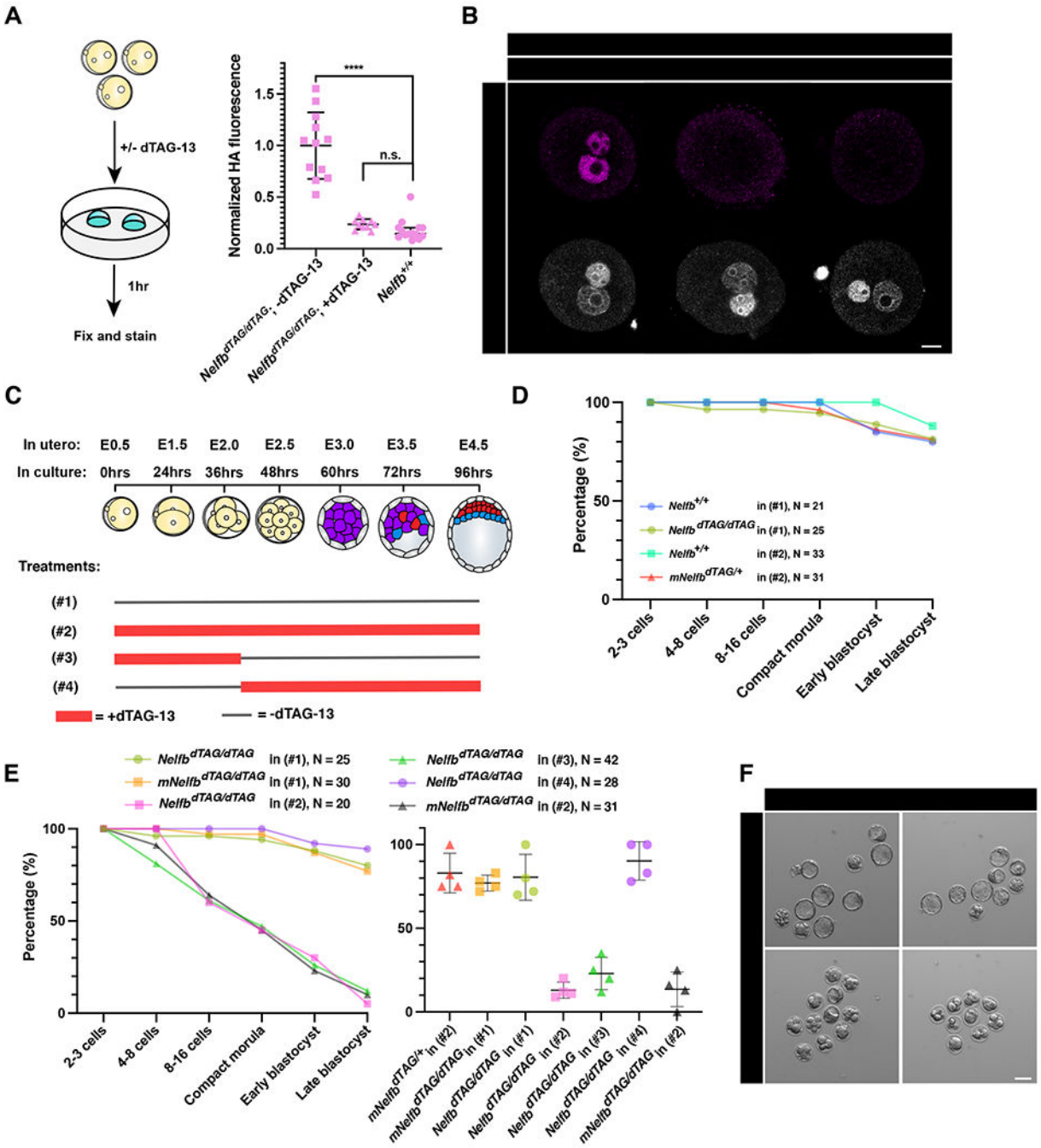

Figure 5.

NELFB is required for pre-implantation development during zygote-2-cell stage.

(A) (Left) Schematic of testing the dTAG system in zygotes. Homozygous *Nelfb*$^{dTAG/dTAG}$ embryos were collected at E0.5 and cultured with or without 500nM dTAG-13 for 1hr. (Right) Quantified mean HA signal in zygotes +/− 1 hr dTAG-13. Each dot represents a pro-nuclei. HA signal is normalized to non-treated embryos.

(B) Immunofluorescence images of zygotes retrieved after 1hr culture +/− dTAG-13. Pro nuclei were labeled with Hoechst. Scale bars, 20μm.

(C) Schematic of culture conditions for following panels D and E, showing when dTAG-13 is added and removed for each condition in zygote to blastocyst culture. The treatment numbers: (#1): no dTAG-13, (#2) constant dTAG-13, (#3) 36hrs dTAG-13 from zygote to 4-cell stage followed by washing, (#4) 60hrs dTAG-13 from 4-cell stage to late blastocyst stage.

(D) Average number of embryos reaching the indicated developmental stage per group/treatment. Control conditions are shown. Figure legends show genotype, treatment regiment, and total number of cultured embryos. *mNlfb* refers to maternal *Nelfb* genotype.

(E) (Left) Average number of embryos reaching the indicated developmental stage per group/treatment. Control conditions are shown. Figure legends show genotype, treatment regiment, and total number of cultured embryos. Testing conditions are shown with littermate controls in each experiment. (Right) plot shows the average number of embryos successfully reaching late blastocyst stage in each separate litter per condition. *mNelfb* refers to maternal *Nelfb* genotype.

(F) Representative images of cultured embryos at hour 96. Scale bars, 50μm.

For all experiments, maximum intensity projection (MIP) is shown in images. Plots show each data point with group mean and interquartile range. Student t-test was used to determine significance. Statistical significance is classified based on p-value as: n.s. > 0.05, * < 0.05, ** < 0.01, *** < 0.001, **** < 0.0001.

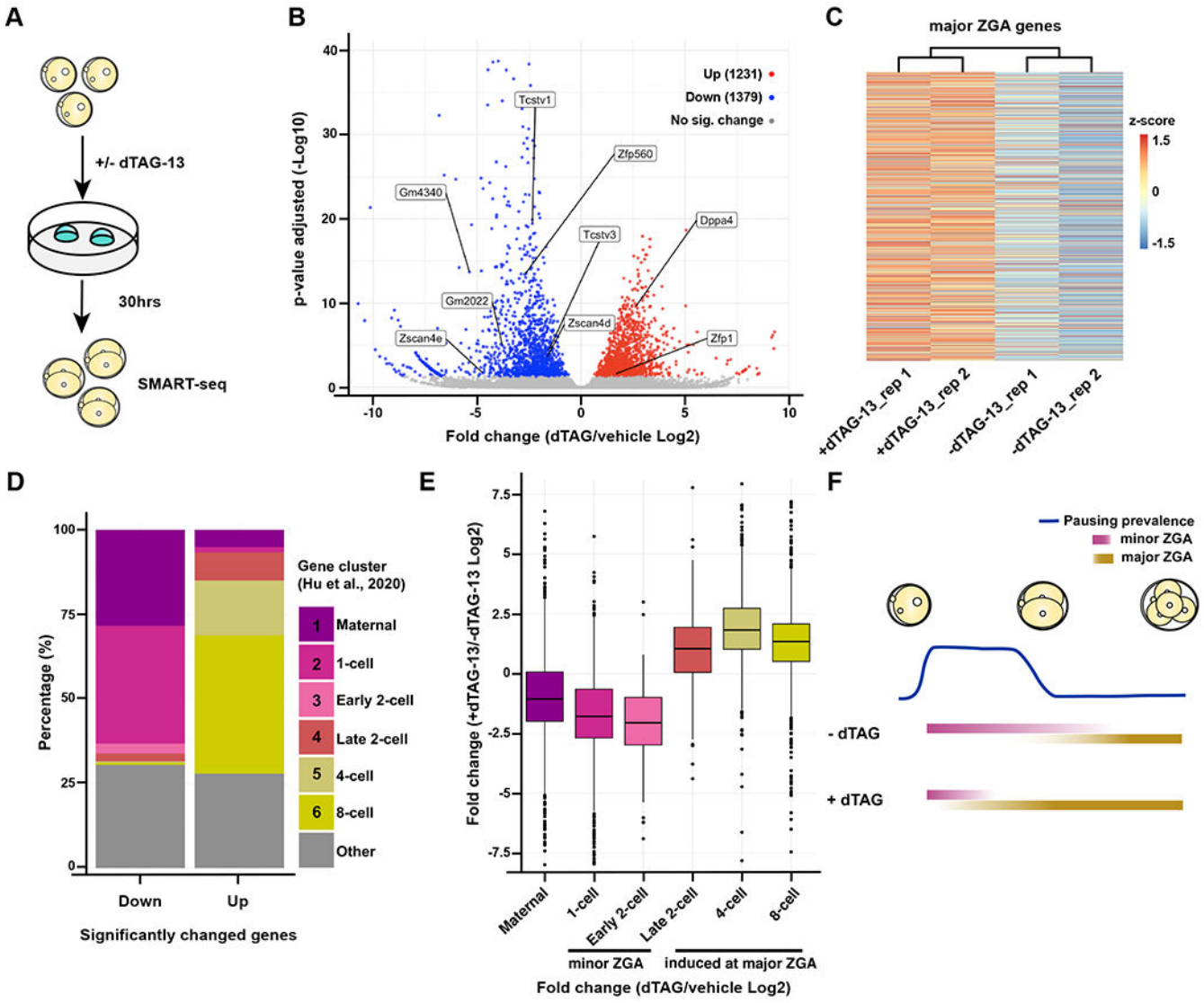

Figure 6.

NELFB facilitates ZGA in mouse development

(A) Schematic of experiment. *Nelfb*$^{dTAG/dTAG}$ zygotes were cultured for 30hrs +/− dTAG-13 to late 2-cell stage, then collected for sequencing using SMART-seq.

(B) Volcano plot of differentially expressed genes determined by DEseq2. P. adj of 0.05 was used as a cutoff.

(C) Heatmap showing z-score of major ZGA genes +/− dTAG-13. 3481 genes are shown representing cluster one from Abe et al., 2018.

(D) Identifying the clusters of up- and downregulated genes using clusters from Hu et al., 2020.

(E) Boxplot showing the overall change of expression levels +/− dTAG-13 in each cluster from Hu et al., 2020.

(F) Working model to explain the results. NELF may serve to stabilize RNA Pol II pausing prior to major ZGA, resulting in major ZGA attenuation.

KEY RESOURCES TABLE

REAGENT or RESOURCE	SOURCE	IDENTIFIER
Antibodies		
Rabbit anti-NANOG	Reprocell	Cat# RCAB001P, RRID: AB_1962694
Goat anti-GATA6	R&D Systems	Cat# AF1700, RRID: AB_2108901
Mouse anti-CDX2	BioGenex	Cat# MU-392AUC, RRID: AB_2650531
Rabbit anti-COBRA1/NELFB	Invitrogen	Cat# PA5-54169, RRID: AB_2639998
Rabbit anti-COBRA1	Cell Signaling	Cat# 14894, RRID: AB_2798637
Mouse anti-HA	Abcam	Cat# ab130275, RRID: AB_11156884
Rabbit anti-HA	Cell Signaling	Cat# 3724, RRID: AB_1549585
Bacterial and Virus Strains		
E. coli DH5a	NEB	C2987I
Chemicals, Peptides, and Recombinant Proteins		
Hoechst 33342	Invitrogen	Cat# H3570
Stemolecule™ CHIR99021	Fisher	Cat# NC9785126
PD0325901	Reprocell	Cat# 04-0006-10
EmbryoMax KSOM (+AA w/o PhenolRed)	Sigma	Cat# MR-106-D
FHM	Millipore	Cat# MR-025-D
Proteinase K	Roche	Cat# 03115801001
16% PFA	Electron microscopy sciences	Cat# 15710
Acid Tyrode’s	Millipore	Cat# MR-004-D
Glycine	Sigma	Cat# G7403
Triton X-100	Sigma	Cat# X100
Horse Serum	Sigma	Cat# H0146
DMEM	Life technologies	Cat# 11995073
NEAA	Life technologies	Cat# 11140-050
Glutamine	Life technologies	Cat# 25030164
Sodium Pyruvate	Life technologies	Cat# 11360070
2-mercaptoethanol	Life technologies	Cat# 21985023
Fetal Calf Serum	VWR	Cat# 97068-085
0.05% Trypsin EDTA	Life technologies	Cat# 25200114
Hyaluronidase	Millipore	Cat# H4272
Gelatine	Millipore	Cat# 104070
Penicillin/Streptomycin	Life technologies	Cat# 15140163
Mitomycin C	Sigma	Cat# M4287
Hoechst 33258, Pentahydrate (bis-Benzimide)	Invitrogen	Catalog No: H3569
Fluoro-Gel	Electron Microscopy Sciences	Catalog No: 17985-10
Sodium azide	Fisher Scientific	Catalog No: S227I-25
Heparin sodium salt	Sigma-Aldrich	Catalog No: H3393-50KU

REAGENT or RESOURCE	SOURCE	IDENTIFIER
Normal donkey serum	Sigma-Aldrich	Catalog No: D9663-10M
Critical Commercial Assays		
NEBuilder HiFi assembly kit	NEB	Cat# E5520S
Pierce™ BCA protein assay kit	Thermo	Cat# 23225
Deposited Data		
RNA-seq data	This manuscript	GSE185099
All source data for figures	Table S2	N/A
Experimental Models: Cell Lines		
Cells: Embryonic stem cell line HK3i	MSK Mouse Genetics Core Facility	(Kiyonari et al., 2010)
Cells: mESC *Nelfb*$^{dTAG/+}$	This manuscript	N/A
Experimental Models: Organisms/Strains		
Mouse: CD1	Charles River Laboratory	Cat# 022
Mouse: *Nelfb*$^{dTAG/+}$	This manuscript	N/A
Oligonucleotides		
Oligonucleotides in Table S1	This manuscript	N/A
Software and Algorithms		
Fiji/Image J	(Schindelin et al., 2012)	https://imagej.nih.gov/ij/
R Studio 1.1.456/R 4.0.2	RStudio, Inc.	https://rstudio.com/
DEseq2 3.13	Bioconductor (Love et al., 2014)	https://bioconductor.org/packages/release/bioc/html/DESeq2.html
ggplot2 3.3.5	R package	https://ggplot2.tidyverse.org
MINS	(Lou et al., 2014)	http://katlab-tools.org/
Prism 9	GraphPad Software	https://www.graphpad.com/scientific-software/prism/
ZEN	Carl Zeiss Microsystems	https://www.zeiss.com/microscopy/us/products/microscope-software/zen.html
Other		
Glass-bottom dish	MatTek	Cat# P35G-1.5-14-C
Nitrocellulose membrane	Cell Signaling	Cat #12369